

Decoding the Multimodal Mind: Generalizable Brain-to-Text Translation via Multimodal Alignment and Adaptive Routing

Chunyu Ye^{1,2}, Yunhao Zhang^{1,2}, Jingyuan Sun³,
Chong Li^{1,2}, Chengqing Zong^{1,2}, Shaonan Wang^{1,2*}

¹State Key Laboratory of Multimodal Artificial Intelligence Systems, Institute of Automation, CAS, Beijing, China

²School of Artificial Intelligence, University of Chinese Academy of Sciences, Beijing, China

³Department of Computer Science, The University of Manchester, UK

Abstract

Decoding language from the human brain remains a grand challenge for Brain-Computer Interfaces (BCIs). Current approaches typically rely on unimodal brain representations, neglecting the brain’s inherently multimodal processing. Inspired by the brain’s associative mechanisms, where viewing an image can evoke related sounds and linguistic representations, we propose a unified framework that leverages Multimodal Large Language Models (MLLMs) to align brain signals with a shared semantic space encompassing text, images, and audio. A router module dynamically selects and fuses modality-specific brain features according to the characteristics of each stimulus. Experiments on various fMRI datasets with textual, visual, and auditory stimuli demonstrate state-of-the-art performance, achieving an 8.48% improvement on the most commonly used benchmark. We further extend our framework to EEG and MEG data, demonstrating flexibility and robustness across varying temporal and spatial resolutions. To our knowledge, this is the first unified BCI architecture capable of robustly decoding multimodal brain activity across diverse brain signals and stimulus types, offering a flexible solution for real-world applications.

1 Introduction

Brain-Computer Interfaces (BCIs) enable users to interact with the external world using only their thoughts. One of the most significant applications of BCIs is language decoding, which aims to translate brain signals into text. This capability holds tremendous promise for restoring communication in individuals with severe language impairments, thereby reconnecting them with their environment. However, reliable language decoding remains exceptionally challenging because the brain representation of thought is inherently complex and multimodal (Meyer et al. 2007; Barsalou 2008; Anderson et al. 2017). For example, reading the sentence “a dog barks in a grassy field” engages not only linguistic processing but also evokes vivid visual and auditory imagery. Consequently, recorded brain signals comprise a rich mixture of linguistic, visual, and auditory representations.

Most existing decoding models, however, exploit only a single modality of these brain representations (Mai and Zhang 2023; Xia et al. 2024; Qiu et al. 2025), learning a direct mapping from brain signals to unimodal representation.

*Corresponding author.

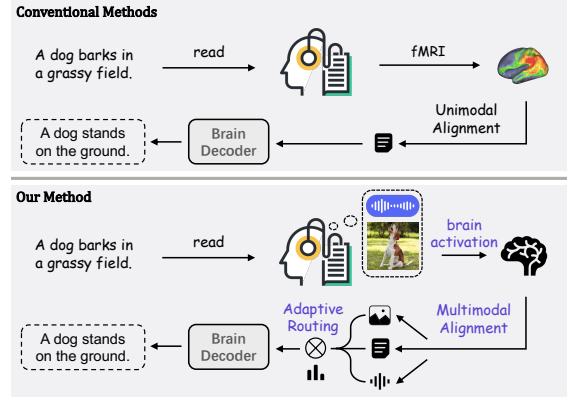


Figure 1: Top: Conventional BCI frameworks decode language from unimodal brain representations. Bottom: Our proposed framework (supports diverse brain signals and stimulus types) leverages multimodal brain representations for language decoding via multimodal alignment and adaptive routing strategy.

This approach overlooks the brain’s inherently multimodal processing: text can evoke visual imagery, and images can activate language-related brain regions (Zhao et al. 2025; Spence 2011; Bolam et al. 2022). Such cross-modal activations provide complementary information that is crucial for more effective brain decoding.

To bridge this gap, we propose a unified BCI decoding framework that leverages multimodal brain activations evoked by unimodal stimuli. As illustrated in Figure 1, our approach performs multimodal alignment by learning a mapping from brain signals to a shared semantic space encompassing text, image, and audio modalities. At the core of our framework is an adaptive routing mechanism that dynamically selects and fuses multimodal brain features for each input, emulating the brain’s associative processes. For each brain sample, this module analyzes the underlying neural representations and determines the optimal contribution of each modality to decode the user’s thoughts.

We evaluate the proposed framework on three widely used functional magnetic resonance imaging (fMRI) datasets containing text, image, and audio stimuli, achieving state-of-the-art performance across all benchmarks. Notably, we

observe an 8.48% improvement on the most commonly used dataset. In contrast to previous approaches that are limited to a single dataset or neuroimaging modality, our model demonstrates strong generalizability. We extend the framework to electroencephalography (EEG) and magnetoencephalography (MEG) data, which offer high temporal resolution compared to the high spatial resolution of fMRI, and consistently observe superior performance. Our contributions are summarized as follows:

- We propose a unified BCI decoding framework that maps brain signals to a shared semantic space across text, image, and audio modalities, enabling effective and scalable brain decoding.
- We introduce a modality routing mechanism that dynamically adjusts the contribution of textual, visual, and auditory representations on a per-sample basis.
- We evaluate the proposed framework across multiple neuroimaging modalities (fMRI, EEG, and MEG) and multiple stimuli (vision, language, and audio), achieving state-of-the-art performance and demonstrating robustness and generalizability.

Together, our work presents the first unified and scalable solution for decoding the brain’s multimodal representations, advancing toward more robust, adaptive, and general-purpose brain-computer interfaces.

2 Related work

This study focuses on decoding text from brain signals (e.g., fMRI) by leveraging the multimodal representation capabilities of a Multimodal Large Language Model (MLLM). The following sections will respectively introduce related work in brain-conditioned text decoding and MLLMs.

Brain-Conditioned Text Decoding is a key component of BCIs, aiming to reconstruct text from brain signals. Early research primarily employed fMRI due to its high spatial resolution and non-invasive nature. These pioneering efforts often utilized classification tasks to extract semantic information from fMRI data (Mitchell et al. 2008; Palatucci et al. 2009), such as predicting target words from neural signals using contextual prompts (Zou et al. 2022). With the advent of large language models (LLMs), fMRI decoding has evolved from a classification paradigm to a continuous generation paradigm. Approaches in this new paradigm include methods that reconstruct text by directly comparing brain-predicted and candidate text embeddings (Tang et al. 2023; Zhao et al. 2024). Furthermore, Ye et al. (2025) proposed a method for continuous text decoding by employing fMRI embeddings as a prefix to guide the text generation process.

Moreover, breakthroughs in MLLMs have further expanded the capabilities of fMRI decoding by leveraging additional image information. Huang et al. (2025) utilized contrastive learning to align fMRI signals with multimodal (text and image) representations, employing a cross-attention model to effectively decode neural signals. Similarly, Xia et al. (2024) aligned fMRI embeddings with image embeddings to leverage the native image-understanding capabilities of MLLMs, further demonstrating the efficacy of integrating multimodal models into fMRI decoding. However,

prior work has often focused on single-stimulus fMRI decoding and faced challenges in effectively utilizing auxiliary information from multiple modalities to aid fMRI decoding.

Meanwhile, decoding efforts based on MEG and EEG data have also been actively pursued. In recent years, researchers have begun harnessing the powerful representational and generalization capabilities of LLMs to enhance MEG/EEG decoding, enabling more accurate mapping of neural signals to linguistic outputs (Yang et al. 2024b; Liu et al. 2024; Duan et al. 2023). However, most of these studies focus exclusively on a single type of brain signal and rely solely on unimodal representations, which limits both the generalizability of BCIs and the accuracy of decoding. Here, we propose a unified model that processes brain signals from fMRI, MEG, and EEG by aligning brain embeddings with multimodal embeddings to generate coherent text.

Multimodal Large Language Models are designed to process and understand multimodal information through various pretraining tasks such as contrastive learning, masked language modeling, and image-text matching. Most work in this area has focused on image and text. Flamingo (Alayrac et al. 2022) was an early attempt that infused frozen visual features into LLMs via cross-attention, enabling the model to achieve excellent performance across various multimodal benchmarks. BLIP-2 (Li et al. 2023) introduced a lightweight Q-Former to summarize image features into compact tokens aligned with the language model input. With the rise of instruction-following LLMs, models like Qwen2-VL (Wang et al. 2024) connect a pre-trained CLIP-ViT (Radford et al. 2021) and a Qwen LLM (Yang et al. 2024a) through a linear layer, enabling it to follow visual instructions and perform general-purpose visual and language understanding.

Recent efforts have extended beyond vision to include additional modalities such as audio and video. Qwen2.5-Omni (Xu et al. 2025), for example, is a streaming end-to-end multimodal model that integrates text, image, audio, and video using block-wise encoding and time-aligned position embeddings for synchronized cross-modal understanding and generation. Other efforts, such as OneLLM (Han et al. 2024), have begun exploring unconventional modalities like point clouds and fMRI. However, these models typically require significant computational resources and large-scale training data. In this work, we leverage Qwen2.5-Omni’s multimodal representation capabilities and introduce an efficient alignment strategy that enables learning from minimal supervision with only a few training examples.

3 Method

We propose a unified brain decoder, as illustrated in Figure 2, which achieves high-performance text decoding through multimodal alignment and adaptive routing strategy. In this section, we present the overall model architecture (Sec. 3.1), and describe the two training phases: multimodal instruction tuning (Sec. 3.2) and projectors fusion (Sec. 3.3). During training, the decoder aligns brain signals with associated auxiliary multimodal information, while during inference, it directly generates text from brain signals.

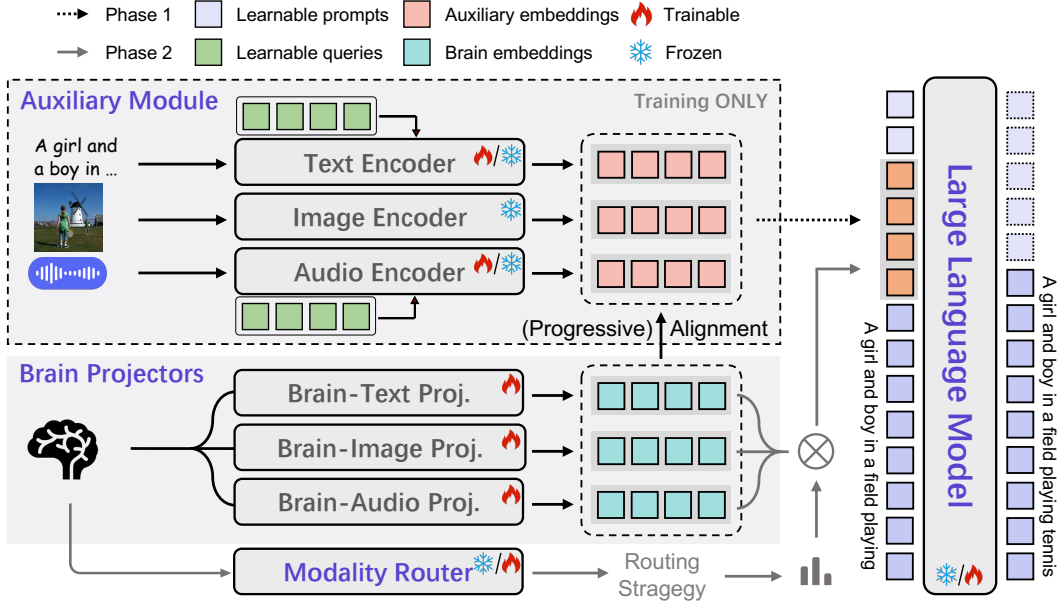


Figure 2: Architecture of the proposed BCI framework, consisting of four key components: an Auxiliary Module (providing auxiliary embeddings for alignment during training), Brain Projectors (for brain feature extraction), a Modality Router (for fusing multimodal brain features), and an LLM (for text generation). Training involves two phases: (1) Multimodal Instruction Tuning: The Auxiliary Module is trained to produce modality-specific embeddings for multimodal captioning, with Brain Projectors concurrently trained to align them; (2) Projectors Fusion: the Modality Router learns to dynamically combine projector outputs for LLM-driven text generation. During inference, brain signals (fMRI, EEG, or MEG) are directly projected into the multimodal brain embeddings and fused to generate coherent text without any auxiliary information.

3.1 Core components

Auxiliary Module generates modality-specific embeddings from image, text, or audio inputs, which are then utilized by the LLM for multimodal captioning. Concurrently, these embeddings also serve as auxiliary embeddings for training the Brain Projectors. The text encoder employs a transformer architecture with a cross-attention module, where learnable queries attend to pre-trained text embeddings (keys/values) to yield a fixed-length vector. The image encoder, based on CLIP-ViT (Radford et al. 2021), extracts effective semantic information. The audio encoder combines Whisper-large-v3 (Radford et al. 2023) with a cross-attention module to transform audio signals via learnable queries into fixed-length vectors. All three modalities produce embeddings of identical dimensionality within a unified representation space, facilitating Brain Projectors alignment. This module is exclusively used during training to enhance alignment and is not employed during inference.

Brain Projectors consist of M projectors, denoted $\{P_1, P_2, \dots, P_M\}$, each based on the CLIP-ViT architecture. The number of Brain Projectors matches the M auxiliary modalities processed by the Auxiliary Module, ensuring a one-to-one mapping. Each projector P_i encodes brain signals into distinct embeddings, which is then aligned with the corresponding auxiliary embedding.

Modality Router Unlike previous approaches that treat the brain as unimodal, we introduce the Modality Router, inspired by the brain’s associative processes, which calculates

the contribution of different modalities (e.g., visual, textual, auditory) for each brain sample, leveraging the multimodal nature of brain representation. Given a raw brain sample b , the Modality Router \mathcal{R} assigns a weight w_i to each Brain Projector P_i , facilitating the dynamic integration of multimodal information. We propose three distinct routing strategies for the Modality Router, as illustrated in Figure 3.

The soft merge strategy, shown in Figure 3(a), constructs the router as a multi-layer perceptron (MLP). The brain sample b is fed through the MLP and a subsequent softmax function to yield a probability distribution over the modalities.

In contrast, the hard select strategy, depicted in Figure 3(b), selects the single most relevant modality for each brain sample. Like the soft merge strategy, it employs an MLP; however, to enable differentiable hard selection during training, we employ the Gumbel-Softmax function (Jang, Gu, and Poole 2016). Specifically, given the logits $\mathbf{l} = \text{MLP}(b)$, the hard selection is approximated by:

$$y_i = \text{softmax} \left(\frac{\log l_i + g_i}{\tau} \right), \quad (1)$$

where l_i denotes the i -th logit, $g_i \sim \text{Gumbel}(0, 1)$, and $\tau > 0$ is a temperature hyperparameter that controls the sharpness of the distribution. A Top-1 selection is then applied to transform the continuous vector \mathbf{y} into a one-hot weight vector \mathbf{w} :

$$w_i = \begin{cases} 1, & i = \arg \max_j y_j, \\ 0, & \text{otherwise.} \end{cases} \quad (2)$$

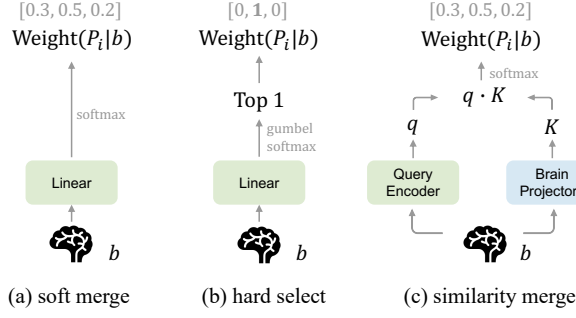


Figure 3: Comparison of three routing strategies for calculating Brain Projector importance weights. (a) Soft merge: a linear layer with Softmax calculates weights for all projectors. (b) Hard select: a linear layer with Gumbel-Softmax selects the top-scoring projector. (c) Similarity merge: dot-product similarities between the query and brain embeddings are Softmax-normalized to serve as weights.

During backpropagation, gradients are computed with respect to the continuous values \mathbf{y} , enabling end-to-end optimization via the *straight-through estimator*. This approach allows the model to make discrete modality selections while preserving differentiability.

Finally, the similarity merge strategy (Figure 3(c)) utilizes an attention mechanism to assign modality weights. A query encoder processes the raw brain signal b to produce a query vector q . Concurrently, the Brain Projectors provide their respective multimodal brain embeddings $P_i(b)$, forming the key set $K = \{k_1, k_2, \dots, k_M\}$. The weight w_i for each modality is obtained from the similarity between the query vector q and each modality’s key vector k_i , computed using the dot product followed by softmax normalization $w_i = \text{softmax}(q \cdot k_i)$. This procedure yields context-sensitive modality weights that capture the learned relevance of each representation to the brain-derived query.

All three routing strategies ultimately compute weights w_i for each projector, which are then used to fuse the multimodal brain embeddings as

$$H = \sum w_i P_i(b). \quad (3)$$

LLM We adopt the language decoder of Qwen2.5-Omni (Xu et al. 2025) as the LLM. Its input is a sequence of learnable soft-prompt tokens followed by either a brain or modality embedding. The soft-prompt is initialized using pre-trained embeddings derived from instruction text. This approach is motivated by studies suggesting that soft prompts aligned with the pre-trained embedding distribution of the LLM tend to facilitate more effective convergence and enhanced performance (Lester, Al-Rfou, and Constant 2021).

3.2 Multimodal Instruction Tuning

We first employ prompt tuning to optimize the modality encoders within the Auxiliary Module. This process extracts fixed-length, modality-specific embeddings that serve as auxiliary embeddings. Subsequently, the Brain Projectors

align the brain-derived embeddings to these auxiliary embeddings, ensuring effective cross-modal correspondence.

The Auxiliary Module is optimized to produce modality-specific embeddings that, when fed into the LLM, enable multimodal captioning. Specifically, given auxiliary information paired with brain signals, the LLM is required to generate the corresponding textual description. Concretely, for the image modality it performs standard image captioning; for text, input re-paraphrasing; and for audio, speech transcription. This objective encourages each encoder to learn semantically rich representations aligned with the LLM’s embedding space. The captioning loss is defined as

$$\mathcal{L}_{\text{cap}} = - \sum_{k=1}^T \log P_{\theta}(t_k | t_{<k}, [S; z_m]), \quad (4)$$

where T is the target length, t_k the k -th token with prefix $t_{<k}, [S; z_m]$ the concatenation of soft-prompt S and modality embedding z_m , and P_{θ} the LLM’s distribution.

Once the Auxiliary Module produces embeddings sufficient for multimodal captioning, we transfer this knowledge to the Brain Projectors through alignment. We employ Mean Squared Error (MSE) for this purpose. The alignment loss encourages each brain embedding z_b to match its corresponding modality-specific auxiliary embedding z_m :

$$\mathcal{L}_{\text{align}} = \mathbb{E}_{(z_b, z_m) \sim \mathcal{D}} [\|z_b - z_m\|_2^2]. \quad (5)$$

Although the image encoder is pre-aligned to the LLM space, the text and audio encoders are randomly initialized and require training to produce effective embeddings. Therefore, we employ a dynamic weighting scheme for progressive alignment:

$$\alpha(t) = \frac{1}{1 + e^{-\lambda(t-t_0)}}, \quad (6)$$

where λ controls the transition sharpness, t_0 denotes the midpoint step, and t is the current training iteration.

Ultimately, we jointly minimize the captioning and alignment losses according to a progressive schedule:

$$\mathcal{L}(t) = \mathcal{L}_{\text{cap}} + \alpha(t) \mathcal{L}_{\text{align}}. \quad (7)$$

At the start of training, $\alpha(t) \approx 0$ biases optimization towards multimodal captioning; as t increases, $\alpha(t) \rightarrow 1$ gradually shifts focus to encoder-projector alignment. Upon completion, brain and auxiliary embeddings are well aligned within the LLM’s representation space.

3.3 Projectors Fusion

After Multimodal Instruction Tuning aligns brain embeddings with specific modalities, this phase seeks to effectively fuse these embeddings to better leverage the multimodal nature of brain signals. We route brain signals through a Modality Router to compute contribution scores w_i for each modality, then weight the Brain Projector outputs $P_i(b)$ to obtain a unified embedding (see Eq. (3)).

This multimodal embedding, H , is subsequently passed into the LLM for language modeling.

To prevent overfitting to a single projector and promote balanced training, we introduce a sample-level load balancing strategy for both merge-based routers (soft and similarity merge) and select-based routers (hard select):

$$\mathcal{L}_{\text{load}} = \begin{cases} -\frac{1}{N} \sum_{i=1}^N \sum_{k=1}^M \log w_{i,k}, & (\text{merge-based}) \\ M \sum_{k=1}^M f_k P_k, & (\text{select-based}) \end{cases} \quad (8)$$

where N is the batch size, M the number of projectors, and $w_{i,k}$ the weight assigned to projector k . For merge-based routers, the logarithmic term prevents any projector’s weight from vanishing. For select-based routers, we define:

$$f_k = \frac{1}{N} \sum_{i=1}^N \mathbb{I}[\text{proj}(b_i) = k], \quad P_k = \frac{1}{N} \sum_{i=1}^N w_{i,k}, \quad (9)$$

where f_k is the fraction of samples routed to projector k and P_k its average gating probability. Thus, the merge-based term maximizes the product of total weights across projectors, while the select-based term aligns empirical routing frequencies f_k with gating probabilities P_k .

Through the load balancing loss, the brain router can more comprehensively utilize the multimodal brain representations. To prevent the distribution differences from expanding further in this training step, we still introduce the alignment loss to regularize the distribution of the brain embeddings. The final loss is

$$\mathcal{L} = \mathcal{L}_{\text{cap}} + \lambda_1 \mathcal{L}_{\text{align}} + \lambda_2 \mathcal{L}_{\text{balance}}, \quad (10)$$

where λ_1 and λ_2 are hyperparameters that weight the alignment loss $\mathcal{L}_{\text{align}}$ and the load balancing loss $\mathcal{L}_{\text{balance}}$, respectively.

4 Experimental Setup

4.1 Datasets

For the fMRI data, we utilized three different modality-specific datasets induced by visual (NSD), textual (Pereira), and auditory (Huth) stimuli. The NSD dataset (Allen et al. 2022) provides paired fMRI and image data based on COCO stimuli, using standard train/test splits (Huang et al. 2025; Xia et al. 2024). The Pereira dataset (Pereira et al. 2018) comprises fMRI recordings collected while participants read encyclopedic sentences; each continuous scan captures brain activity elicited by multiple words simultaneously. The Huth’s dataset (LeBel et al. 2023) contains fMRI data from 8 participants listening to 27 natural narrative stories, with official preprocessing applied.

The MEG dataset (Wang et al. 2022) comprises recordings from 12 participants listening to 60 stories, segmented into nine overlapping 200 ms windows over the first second after each word offset. The ZuCo2 EEG dataset (Zou et al. 2022) includes EEG responses from 18 participants to 739 Wikipedia sentences (349 in normal reading; 390 in task-specific reading). More details about the datasets are provided in the appendix.

4.2 Baselines

For the NSD dataset, we compare models trained solely on single-subject data to ensure a fair evaluation. The following baselines are considered: SDRecon (Takagi and Nishimoto 2023), UniBrain (Mai and Zhang 2023), and BrainCap (Ferrante et al. 2023), which primarily utilize linear regression to map fMRI to LLM input space. OneLLM (Han et al. 2024) stands out as an MLLM that aligns fMRI, alongside seven other modalities, with language. BrainChat (Huang et al. 2025) employs contrastive cross-attention to align fMRI with text. UMBRAE (Xia et al. 2024) maps fMRI embeddings into the same space as image embeddings to leverage MLLMs’ native image-understanding capabilities. MindLLM (Qiu et al. 2025) employs a neuroscience-informed attention mechanism for fMRI decoding. Notably, all baseline methods consider only unimodal brain representations, whereas our model effectively exploits the brain’s multimodal capabilities.

For all other datasets, most of the methods mentioned above were not applied due to their heavy reliance on visual stimuli. Instead, we establish a lower bound by using randomly selected brain signals. We also implement a simple baseline that encodes brain signals with a ViT encoder followed by a linear layer before feeding them into an LLM. Furthermore, BrainLLM (Ye et al. 2025) serves as a key baseline thanks to its intuitive, generalizable framework. For the Huth dataset, we include an additional competitive baseline proposed by Tang et al. (2023).

4.3 Metrics

We evaluate the generated captions using standard text-based metrics, including BLEU- k (Papineni et al. 2002), METEOR (Banerjee and Lavie 2005), ROUGE (Lin 2004), CIDEr (Vedantam, Lawrence Zitnick, and Parikh 2015), and word error rate (WER). For datasets with reference images, we additionally assess caption–image relevance using CLIP-S and RefCLIP-S (Hessel et al. 2021). Together, these metrics provide a comprehensive assessment of both linguistic fidelity and visual alignment.

4.4 Implementation Details

Each projector was initialized with a pre-trained CLIP ViT-L/14 backbone, and the Qwen2.5-Omni 7B model served as the language decoder. During multimodal instruction tuning, the number of learnable soft prompt tokens was set to 10, and the length of learnable queries was fixed at 16. All input images were uniformly resized to $112 \times 112 \times 3$ pixels. In the subsequent projectors fusion phase, the loss weights for alignment and language modeling were both set to 1, while the load balancing loss weight was set to 0.01. We employed the AdamW optimizer with $\beta_1 = 0.9$, $\beta_2 = 0.999$, a learning rate of 5×10^{-5} , and a batch size of 32 in both training phases. We used FLUX.1-dev with a guidance scale of 3.5 for auxiliary image generation. All experimental procedures are carried out using four NVIDIA Tesla V100 GPUs.

Method	BLEU-1	BLEU-2	BLEU-3	BLEU-4	METEOR	ROUGE-L	CIDEr	CLIP-S	RefCLIP-S
SDRecon	36.21	17.11	7.22	3.43	10.03	25.13	13.83	61.07	66.36
OneLLM	47.04	26.97	15.49	9.51	13.55	35.05	22.99	54.80	61.28
UniBrain	-	-	-	-	16.90	22.20	-	-	-
BrainCap	55.96	36.21	22.70	14.51	16.68	40.69	41.30	<u>64.31</u>	69.90
BrainChat	52.30	29.20	17.10	10.70	14.30	45.70	26.10	-	-
UMBRAE	57.63	38.02	25.00	16.76	18.41	42.15	51.93	66.44	72.12
MindLLM	58.05	37.95	24.40	16.14	16.62	42.03	43.04	-	-
Ours (soft merge)	<u>61.46</u>	<u>43.37</u>	<u>30.07</u>	<u>21.04</u>	<u>20.60</u>	<u>46.15</u>	<u>63.68</u>	62.72	69.72
Ours (hard select)	<u>60.69</u>	<u>42.59</u>	<u>29.90</u>	<u>21.33</u>	<u>19.67</u>	<u>45.66</u>	<u>59.55</u>	60.31	67.75
Ours (similarity merge)	61.53	43.45	30.21	21.92	20.71	46.45	63.88	63.13	<u>70.12</u>

Table 1: Results of brain captioning on NSD subject 1. *Soft merge*, *hard select*, and *similarity merge* refer to the three routing strategies illustrated in Figure 3.

Dataset	Method	with text prompt				without text prompt			
		BLEU-1↑	ROUGE-1↑	ROUGE-L↑	WER↓	BLEU-1↑	ROUGE-1↑	ROUGE-L↑	WER↓
Pereira	random	31.29	24.15	24.01	83.38	7.87	5.53	5.40	97.26
	linear	32.48	25.21	25.13	82.15	9.21	7.12	7.04	96.92
	BrainLLM	<u>33.51</u>	<u>26.99</u>	<u>26.38</u>	<u>81.03</u>	<u>10.25</u>	<u>7.88</u>	<u>7.49</u>	<u>96.10</u>
	Ours	36.24	27.67	27.54	79.48	14.91	8.21	8.09	96.01
Huth	random	14.89	13.37	13.24	93.35	9.60	8.17	7.79	97.03
	linear	15.32	14.12	14.21	93.01	9.62	8.17	7.81	97.11
	Tang et al. (2023)	14.95	13.39	13.26	93.34	9.67	8.18	7.88	97.00
	BrainLLM	<u>16.91</u>	15.81	<u>15.03</u>	<u>92.16</u>	<u>13.56</u>	11.60	10.99	<u>95.41</u>
	Ours	17.32	<u>15.68</u>	15.12	91.42	13.97	<u>10.98</u>	<u>10.49</u>	95.29

Table 2: Results of brain captioning on Pereira and Huth dataset. *With text prompt* indicates that in addition to brain embeddings, we also provide textual context as input to the LLM to generate the corresponding text.

5 Results

We evaluated our model on three fMRI datasets and extended its application to MEG and EEG data. Section 5.1 presents the quantitative results. Building on these findings, Section 5.2 examines how our model integrates multiple modalities. Finally, Section 5.3 reports ablation studies on the utilized modalities and framework components. Examples of the model’s decoding results, along with a comparative analysis, are provided in the appendix.

5.1 Quantitative Results

fMRI As shown in Table 1 on the NSD dataset, our model outperforms those trained exclusively on unimodal brain representations, achieving an improvement of 8.48%. This result validates the effectiveness of our framework. UMBRAE achieves the highest performance on the CLIP-based metric, likely due to its direct optimization for brain-image alignment. Consequently, its brain embeddings encode more image-specific information; however, its performance on text-based metrics is comparatively lower. In contrast, our approach yields a more balanced and generally superior average performance.

On both the Pereira and Huth datasets, as shown in the Table 2, our model achieves the best performance across most

metrics compared to all baselines. We further analyzed the scenario in which the text prompt is not provided as contextual input for LLM generation. In this more challenging setting, all metrics decline; however, the performance trends observed with text prompts persist, and our approach still achieves the best results on the majority of metrics.

MEG&EEG We further applied our model to MEG and EEG datasets, achieving the highest performance across all evaluation metrics (see Table 3) and demonstrating superior generalizability and scalability compared to other methods.

Dataset	Method	BLEU-1↑	ROUGE-1↑	ROUGE-L↑	WER↓
MEG	random	15.24	11.46	11.39	93.01
	linear	18.98	14.26	14.38	89.94
	BrainLLM	<u>19.59</u>	<u>14.78</u>	<u>14.32</u>	<u>89.10</u>
	Ours	20.96	16.97	16.58	86.20
EEG	random	16.92	12.01	11.97	92.91
	linear	18.03	13.15	13.28	91.32
	BrainLLM	<u>18.29</u>	<u>13.30</u>	<u>13.22</u>	<u>90.28</u>
	Ours	20.03	15.93	15.65	89.19

Table 3: Results on MEG and EEG dataset.

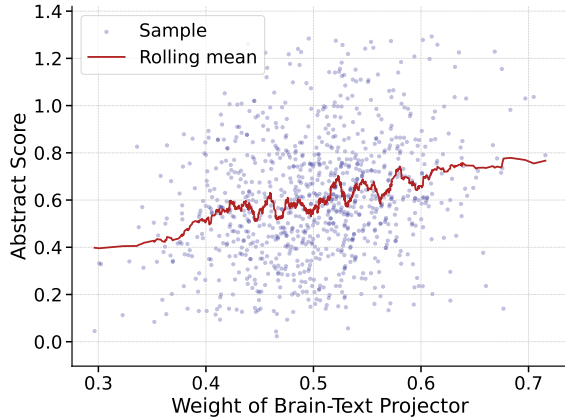


Figure 4: Line-and-scatter plot of Brain-Text Projector weights versus sentence abstractness, displaying individual data points and their rolling mean.

5.2 Analysis

To understand why multimodal brain integration improves performance, we hypothesize that the model captures distinct characteristics of each sample and assigns modality weights accordingly. Specifically, we propose that sentence abstractness governs this weighting: more abstract sentences should receive higher text-modality weights, while more concrete sentences should rely more on visual information. To test this, we analyzed the modality weights for each brain sample in the NSD dataset during decoding.

Figure 4 plots the Brain-Text Projector weight against sentence abstractness, defined as the mean abstractness rating of each word from a predefined dictionary (Brysbaert, Warriner, and Kuperman 2014). Light-blue circles denote individual samples, and the red rolling-mean curve smooths variability, revealing an overall positive trend: higher projector weights correspond to greater abstractness. The Pearson correlation between Brain-Text Projector weight and sentence abstractness is $r = 0.247$ ($p = 0.043$). This significant positive correlation indicates that our model dynamically allocates higher text-modality weights to more abstract sentences during decoding, enhancing interpretability and contributing to its superior performance.

5.3 Ablation Experiments

Utilized Modalities As shown in Table 4, across all datasets, omni models that integrate multimodal brain embeddings outperform any single-modality approach, underscoring the value of cross-modal interactions. Among unimodal variants, vision-based models consistently lead in performance, likely because visual signals offer the richest, most intuitive alignment. In contrast, text-based models trail behind, and audio-based models lag the furthest, suggesting greater difficulty in mapping brain activity to auditory inputs.

Other Components We evaluate the contributions of four essential components—load balancing loss, alignment strategy, two-phase training, and prompt tuning—through ablation studies, as presented in Table 5. The removal of load

Dataset	Modality	BLEU-1↑	ROUGE-1↑	ROUGE-L↑	WER↓
NSD	omni	61.53	46.58	46.45	69.04
	vision	60.57	45.94	45.74	71.39
	text	60.04	45.31	45.65	72.10
Pereira	omni	36.24	27.67	27.54	79.48
	vision	35.23	27.03	26.87	80.31
	text	33.34	26.57	26.21	82.93
Huth	omni	17.32	15.68	15.12	91.42
	audio	16.11	14.19	14.13	93.42
	text	17.01	15.02	15.03	91.87

Table 4: Ablation study of modalities utilized by the framework on NSD, Pereira, and Huth.

Method	BLEU-1	ROUGE-L	CLIP-S
Full model	61.53	46.45	63.13
w/o load balancing loss	52.29	38.18	60.15
w/ KL alignment	59.03	45.19	60.83
w/o progressive alignment	58.78	44.74	60.01
w/o phase 1	40.21	27.39	57.04
w/o phase 2	36.13	24.30	60.38
w/o soft prompts	60.02	45.93	61.59
w/o soft prompt text init	60.23	46.19	62.04

Table 5: Ablation study on framework components on NSD.

balancing loss results in a substantial performance decline, demonstrating its critical role in balancing projector activation. With respect to alignment strategies, we observe that progressive alignment using MSE outperforms KL-based alignment, and omitting alignment altogether leads to further performance degradation. Furthermore, the two-phase training framework is indispensable; eliminating either phase leads to dramatic reductions across all performance metrics, emphasizing the necessity of both stages. Lastly, prompt tuning, especially with soft prompts and text-based initialization, yields modest improvements. Although beneficial, prompt tuning contributes less to overall performance compared to the other components.

6 Conclusion

This paper introduced a novel and generalizable BCI framework that embraces the multimodal nature of brain activity by aligning brain signals with multimodal representations from an MLLM across text, image, and audio domains. A key innovation is our router module, which adaptively selects and fuses modality-specific brain features, mirroring the brain’s associative mechanisms. Extensive evaluations on three fMRI datasets achieved state-of-the-art performance, and the framework showed robustness when extended to EEG and MEG data, consistently achieving superior results across varying temporal and spatial resolutions. This approach brings us closer to real-world applications by enabling BCIs to process diverse input modalities, offering more accurate and flexible systems.

References

- Alayrac, J.-B.; Donahue, J.; Luc, P.; Miech, A.; Barr, I.; Hasson, Y.; Lenc, K.; Mensch, A.; Millican, K.; Reynolds, M.; et al. 2022. Flamingo: a visual language model for few-shot learning. *Advances in neural information processing systems*, 35: 23716–23736.
- Allen, E. J.; St-Yves, G.; Wu, Y.; Breedlove, J. L.; Prince, J. S.; Dowdle, L. T.; Nau, M.; Caron, B.; Pestilli, F.; Charest, I.; et al. 2022. A massive 7T fMRI dataset to bridge cognitive neuroscience and artificial intelligence. *Nature neuroscience*, 25(1): 116–126.
- Anderson, A. J.; Kiela, D.; Clark, S.; and Poesio, M. 2017. Visually grounded and textual semantic models differentially decode brain activity associated with concrete and abstract nouns. *Transactions of the Association for Computational Linguistics*, 5: 17–30.
- Banerjee, S.; and Lavie, A. 2005. METEOR: An automatic metric for MT evaluation with improved correlation with human judgments. In *Proceedings of the acl workshop on intrinsic and extrinsic evaluation measures for machine translation and/or summarization*, 65–72.
- Barsalou, L. W. 2008. Grounded cognition. *Annu. Rev. Psychol.*, 59(1): 617–645.
- Bolam, J.; Boyle, S. C.; Ince, R. A.; and Delis, I. 2022. Neurocomputational mechanisms underlying cross-modal associations and their influence on perceptual decisions. *NeuroImage*, 247: 118841.
- Brysbaert, M.; Warriner, A. B.; and Kuperman, V. 2014. Concreteness ratings for 40 thousand generally known English word lemmas. *Behavior research methods*, 46(3): 904–911.
- Duan, Y.; Zhou, J.; Wang, Z.; Wang, Y.-K.; and Lin, C.-T. 2023. Dewave: Discrete eeg waves encoding for brain dynamics to text translation. *arXiv preprint arXiv:2309.14030*.
- Ferrante, M.; Ozelik, F.; Boccato, T.; VanRullen, R.; and Toschi, N. 2023. Brain captioning: Decoding human brain activity into images and text. *arXiv preprint arXiv:2305.11560*.
- Han, J.; Gong, K.; Zhang, Y.; Wang, J.; Zhang, K.; Lin, D.; Qiao, Y.; Gao, P.; and Yue, X. 2024. Onellm: One framework to align all modalities with language. In *Proceedings of the IEEE/CVF Conference on Computer Vision and Pattern Recognition*, 26584–26595.
- Hessel, J.; Holtzman, A.; Forbes, M.; Bras, R. L.; and Choi, Y. 2021. Clipscore: A reference-free evaluation metric for image captioning. *arXiv preprint arXiv:2104.08718*.
- Huang, W.; Ma, K.; Xie, T.; and Wang, H. 2025. BrainChat: Interactive Semantic Information Decoding from fMRI Using Large-Scale Vision-Language Pretrained Models. In *ICASSP 2025-2025 IEEE International Conference on Acoustics, Speech and Signal Processing (ICASSP)*, 1–5. IEEE.
- Jang, E.; Gu, S.; and Poole, B. 2016. Categorical reparameterization with gumbel-softmax. *arXiv preprint arXiv:1611.01144*.
- LeBel, A.; Wagner, L.; Jain, S.; Adhikari-Desai, A.; Gupta, B.; Morgenthal, A.; Tang, J.; Xu, L.; and Huth, A. G. 2023. A natural language fMRI dataset for voxelwise encoding models. *Scientific Data*, 10(1): 555.
- Lester, B.; Al-Rfou, R.; and Constant, N. 2021. The power of scale for parameter-efficient prompt tuning. *arXiv preprint arXiv:2104.08691*.
- Li, J.; Li, D.; Savarese, S.; and Hoi, S. 2023. Blip-2: Bootstrapping language-image pre-training with frozen image encoders and large language models. In *International conference on machine learning*, 19730–19742. PMLR.
- Lin, C.-Y. 2004. Rouge: A package for automatic evaluation of summaries. In *Text summarization branches out*, 74–81.
- Liu, H.; Hajjaligol, D.; Antony, B.; Han, A.; and Wang, X. 2024. Eeg2text: Open vocabulary eeg-to-text decoding with eeg pre-training and multi-view transformer. *arXiv preprint arXiv:2405.02165*.
- Mai, W.; and Zhang, Z. 2023. Unibrain: Unify image reconstruction and captioning all in one diffusion model from human brain activity. *arXiv preprint arXiv:2308.07428*.
- Meyer, M.; Baumann, S.; Marchina, S.; and Jancke, L. 2007. Hemodynamic responses in human multisensory and auditory association cortex to purely visual stimulation. *BMC neuroscience*, 8(1): 14.
- Mitchell, T. M.; Shinkareva, S. V.; Carlson, A.; Chang, K.-M.; Malave, V. L.; Mason, R. A.; and Just, M. A. 2008. Predicting human brain activity associated with the meanings of nouns. *science*, 320(5880): 1191–1195.
- Palatucci, M.; Pomerleau, D.; Hinton, G. E.; and Mitchell, T. M. 2009. Zero-shot learning with semantic output codes. *Advances in neural information processing systems*, 22.
- Papineni, K.; Roukos, S.; Ward, T.; and Zhu, W.-J. 2002. Bleu: a method for automatic evaluation of machine translation. In *Proceedings of the 40th annual meeting of the Association for Computational Linguistics*, 311–318.
- Pereira, F.; Lou, B.; Pritchett, B.; Ritter, S.; Gershman, S. J.; Kanwisher, N.; Botvinick, M.; and Fedorenko, E. 2018. Toward a universal decoder of linguistic meaning from brain activation. *Nature communications*, 9(1): 963.
- Qiu, W.; Huang, Z.; Hu, H.; Feng, A.; Yan, Y.; and Ying, R. 2025. MindLLM: A Subject-Agnostic and Versatile Model for fMRI-to-Text Decoding. *arXiv preprint arXiv:2502.15786*.
- Radford, A.; Kim, J. W.; Hallacy, C.; Ramesh, A.; Goh, G.; Agarwal, S.; Sastry, G.; Askell, A.; Mishkin, P.; Clark, J.; Krueger, G.; and Sutskever, I. 2021. Learning Transferable Visual Models From Natural Language Supervision. *arXiv:2103.00020*.
- Radford, A.; Kim, J. W.; Xu, T.; Brockman, G.; McLeavey, C.; and Sutskever, I. 2023. Robust speech recognition via large-scale weak supervision. In *International conference on machine learning*, 28492–28518. PMLR.
- Spence, C. 2011. Crossmodal correspondences: A tutorial review. *Attention, Perception, & Psychophysics*, 73(4): 971–995.

Takagi, Y.; and Nishimoto, S. 2023. High-resolution image reconstruction with latent diffusion models from human brain activity. In *Proceedings of the IEEE/CVF conference on computer vision and pattern recognition*, 14453–14463.

Tang, J.; LeBel, A.; Jain, S.; and Huth, A. G. 2023. Semantic reconstruction of continuous language from non-invasive brain recordings. *Nature Neuroscience*, 26(5): 858–866.

Vedantam, R.; Lawrence Zitnick, C.; and Parikh, D. 2015. Cider: Consensus-based image description evaluation. In *Proceedings of the IEEE conference on computer vision and pattern recognition*, 4566–4575.

Wang, P.; Bai, S.; Tan, S.; Wang, S.; Fan, Z.; Bai, J.; Chen, K.; Liu, X.; Wang, J.; Ge, W.; et al. 2024. Qwen2-vl: Enhancing vision-language model’s perception of the world at any resolution. *arXiv preprint arXiv:2409.12191*.

Wang, S.; Zhang, X.; Zhang, J.; and Zong, C. 2022. A synchronized multimodal neuroimaging dataset for studying brain language processing. *Scientific Data*, 9(1): 590.

Xia, W.; de Charette, R.; Oztireli, C.; and Xue, J.-H. 2024. Umbrae: Unified multimodal brain decoding. In *European Conference on Computer Vision*, 242–259. Springer.

Xu, J.; Guo, Z.; He, J.; Hu, H.; He, T.; Bai, S.; Chen, K.; Wang, J.; Fan, Y.; Dang, K.; et al. 2025. Qwen2. 5-omni technical report. *arXiv preprint arXiv:2503.20215*.

Yang, A.; Yang, B.; Hui, B.; Zheng, B.; Yu, B.; Zhou, C.; Li, C.; Li, C.; Liu, D.; Huang, F.; Dong, G.; Wei, H.; Lin, H.; Tang, J.; Wang, J.; Yang, J.; Tu, J.; Zhang, J.; Ma, J.; Yang, J.; Xu, J.; Zhou, J.; Bai, J.; He, J.; Lin, J.; Dang, K.; Lu, K.; Chen, K.; Yang, K.; Li, M.; Xue, M.; Ni, N.; Zhang, P.; Wang, P.; Peng, R.; Men, R.; Gao, R.; Lin, R.; Wang, S.; Bai, S.; Tan, S.; Zhu, T.; Li, T.; Liu, T.; Ge, W.; Deng, X.; Zhou, X.; Ren, X.; Zhang, X.; Wei, X.; Ren, X.; Liu, X.; Fan, Y.; Yao, Y.; Zhang, Y.; Wan, Y.; Chu, Y.; Liu, Y.; Cui, Z.; Zhang, Z.; Guo, Z.; and Fan, Z. 2024a. Qwen2 Technical Report. *arXiv:2407.10671*.

Yang, Y.; Jo, H.; Duan, Y.; Zhang, Q.; Zhou, J.; Lee, W. H.; Xu, R.; and Xiong, H. 2024b. Mad: Multi-alignment meg-to-text decoding. *arXiv preprint arXiv:2406.01512*.

Ye, Z.; Ai, Q.; Liu, Y.; de Rijke, M.; Zhang, M.; Lioma, C.; and Ruotsalo, T. 2025. Generative language reconstruction from brain recordings. *Communications Biology*, 8(1): 346.

Zhao, X.; Sun, J.; Wang, S.; Ye, J.; Zhang, X.; and Zong, C. 2024. Mapguide: A simple yet effective method to reconstruct continuous language from brain activities. *arXiv preprint arXiv:2403.17516*.

Zhao, Y.; Dong, G.; Zhu, L.; and Ying, X. 2025. Memory recall: Retrieval-Augmented mind reconstruction for brain decoding. *Information Fusion*, 103280.

Zou, S.; Wang, S.; Zhang, J.; and Zong, C. 2022. Cross-modal cloze task: A new task to brain-to-word decoding. In *Findings of the Association for Computational Linguistics: ACL 2022*, 648–657.